

JUN 15 1976

AEDC-TR-75-153

Cy. 2



**HEAT-TRANSFER TESTS OF A 0.0175-SCALE MODEL
OF THE SPACE SHUTTLE AT MACH NUMBERS
2.5, 3.5, 4.5, AND 5.5**

**VON KÁRMÁN GAS DYNAMICS FACILITY
ARNOLD ENGINEERING DEVELOPMENT CENTER
AIR FORCE SYSTEMS COMMAND
ARNOLD AIR FORCE STATION, TENNESSEE 37389**

June 1976

Final Report for Period March 31 — May 21, 1975

Approved for public release; distribution unlimited.

Property of U. S. Air Force
AEDC LIBRARY
F40600-75-0-0001

Prepared for

**NATIONAL AERONAUTICS AND SPACE ADMINISTRATION (JSC)
HOUSTON, TEXAS 77058**

NOTICES

When U. S. Government drawings specifications, or other data are used for any purpose other than a definitely related Government procurement operation, the Government thereby incurs no responsibility nor any obligation whatsoever, and the fact that the Government may have formulated, furnished, or in any way supplied the said drawings, specifications, or other data, is not to be regarded by implication or otherwise, or in any manner licensing the holder or any other person or corporation, or conveying any rights or permission to manufacture, use, or sell any patented invention that may in any way be related thereto.

Qualified users may obtain copies of this report from the Defense Documentation Center.

References to named commercial products in this report are not to be considered in any sense as an endorsement of the product by the United States Air Force or the Government.

This report has been reviewed by the Information Office (OI) and is releasable to the National Technical Information Service (NTIS). At NTIS, it will be available to the general public, including foreign nations.

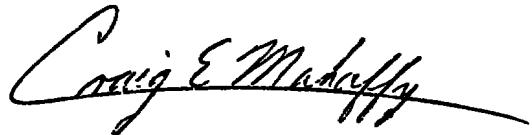
APPROVAL STATEMENT

This technical report has been reviewed and is approved for publication.

FOR THE COMMANDER



CARL J. SCHULZE
Major, USAF
Chief Air Force Test Director, VKF
Directorate of Test



CRAIG E. MAHAFFY
Colonel, USAF
Director of Test

UNCLASSIFIED

REPORT DOCUMENTATION PAGE		READ INSTRUCTIONS BEFORE COMPLETING FORM								
1 REPORT NUMBER AEDC-TR-75-153	2 GOVT ACCESSION NO.	3 RECIPIENT'S CATALOG NUMBER								
4 TITLE (and Subtitle) HEAT-TRANSFER TESTS OF A 0.0175-SCALE MODEL OF THE SPACE SHUTTLE AT MACH NUMBERS 2.5, 3.5, 4.5, AND 5.5		5 TYPE OF REPORT & PERIOD COVERED Final Report-March 31 - May 21, 1975								
		6 PERFORMING ORG. REPORT NUMBER								
7 AUTHOR(s) K. W. Nutt and W. R. Martindale, ARO, Inc.		8. CONTRACT OR GRANT NUMBER(s)								
9 PERFORMING ORGANIZATION NAME AND ADDRESS Arnold Engineering Development Center (XO) Air Force Systems Command Arnold Air Force Station, Tennessee 37389		10 PROGRAM ELEMENT, PROJECT, TASK AREA & WORK UNIT NUMBERS Program Element 921E Project 9772								
11 CONTROLLING OFFICE NAME AND ADDRESS National Aeronautics and Space Administration-JSC (ES3) Houston, Texas 77058		12 REPORT DATE June 1976								
		13 NUMBER OF PAGES 33								
14 MONITORING AGENCY NAME & ADDRESS (if different from Controlling Office)		15 SECURITY CLASS. (of this report) UNCLASSIFIED								
		15a DECLASSIFICATION/DOWNGRADING SCHEDULE N/A								
16 DISTRIBUTION STATEMENT (of this Report) Approved for public release; distribution unlimited.										
17 DISTRIBUTION STATEMENT (of the abstract entered in Block 20, if different from Report)										
18 SUPPLEMENTARY NOTES Available in DDC										
19 KEY WORDS (Continue on reverse side if necessary, and identify by block number) <table style="width: 100%; border: none;"> <tr> <td style="width: 50%;">heat transfer</td> <td style="width: 50%;">Mach numbers</td> </tr> <tr> <td>test methods</td> <td>Reynolds number</td> </tr> <tr> <td>scale model</td> <td>solid rocket booster</td> </tr> <tr> <td>Space Shuttle Integrated Vehicle</td> <td>trajectories (ascent)</td> </tr> </table>			heat transfer	Mach numbers	test methods	Reynolds number	scale model	solid rocket booster	Space Shuttle Integrated Vehicle	trajectories (ascent)
heat transfer	Mach numbers									
test methods	Reynolds number									
scale model	solid rocket booster									
Space Shuttle Integrated Vehicle	trajectories (ascent)									
20 ABSTRACT (Continue on reverse side if necessary and identify by block number) <p style="text-align: center;">Heat-transfer tests were conducted on the Space Shuttle Integrated Vehicle to investigate heat-transfer rates during the ascent phase of the flight profile. The model was a 0.0175-scale, thin skin, thermocouple-equipped model (60-OTS) of the Rockwell International Vehicle 5 configuration. The tests were conducted at nominal Mach numbers of 2.5, 3.5, 4.5, and 5.5 and a free-stream unit Reynolds number of 5 million per foot. Two nose</p>										

UNCLASSIFIED

UNCLASSIFIED

20. ABSTRACT (Continued)

configurations were tested on the external tank. Data were obtained with the external tank alone and with the external tank and solid rocket booster in the integrated vehicle configuration. This report presents representative test results and data comparisons with theoretical calculations.

PREFACE

The work reported herein was conducted by the Arnold Engineering Development Center (AEDC), Air Force Systems Command (AFSC), under the sponsorship of the National Aeronautics and Space Administration, Manned Spacecraft Center (NASA/MSC), for Rockwell International, Downey, California, under Program Element 921E, Project 9772. The results were obtained by ARO, Inc. (a subsidiary of Sverdrup & Parcel and Associates, Inc.), contract operator of AEDC, AFSC, Arnold Air Force Station, Tennessee. The work was done under ARO Project Number V41A-A4A. The authors of this report were K. W. Nutt and W. R. Martindale, ARO, Inc. The final data package was completed on June 13, 1975, and the manuscript (ARO Control No. ARO-VKF-TR-75-141) was submitted for publication on September 12, 1975.

The authors wish to express their appreciation to S. S. Baker, ARO, Inc., for his assistance with the test program and the data analysis.

CONTENTS

	<u>Page</u>
1.0 INTRODUCTION	5
2.0 APPARATUS	
2.1 Wind Tunnel	5
2.2 Model	5
2.3 Instrumentation and Measurement Precision	6
3.0 PROCEDURE	
3.1 Test Conditions	7
3.2 Test Procedure	7
3.3 Data Reduction and Precision	8
4.0 RESULTS AND DISCUSSION	
4.1 External Tank Alone	10
4.2 Integrated Model	11
5.0 CONCLUDING REMARKS	
5.1 External Tank Alone	11
5.2 Integrated Model	12
REFERENCES	12

ILLUSTRATIONS

Figure

1. Schematic View of Tunnel A	15
2. Model Sketch	16
3. Photograph of Integrated Space Shuttle Model	17
4. External Tank Nose Tip Configurations	18
5. Photograph of the Boundary-Layer Trip on the External Tank	19
6. Photograph of External Tank with Nipple Nose	20
7. Typical Data for a Thermocouple	21
8. Heat-Transfer-Rate Distributions for External Tank with Smooth Nose	22
9. Influence of Boundary-Layer Trip on the Heat-Transfer-Rate Distribution of the External Tank with Nipple Nose	23
10. Heat-Transfer-Rate Distributions for the External Tank with Nipple Nose	24

<u>Figure</u>	<u>Page</u>
11. Heat-Transfer-Rate Distributions for the External Tank with Interaction from the Orbiter	26
12. Model Flow-Field Shadowgraphs	28
13. Heat-Transfer-Rate Distribution on the Side of the External Tank with Interaction from the Solid Rocket Booster	30

TABLE

1. Test Matrix	31
NOMENCLATURE	32

1.0 INTRODUCTION

The present tests were conducted to obtain heat-transfer-rate data on the Space Shuttle Integrated Vehicle at simulated ascent flight conditions. The components of the vehicle produce a complex flow field with many shock interactions. Although progress has been made in analyzing shock interference heating (Ref. 1), experimental data are still relied upon to provide vehicle design information. One technique resulting from analytical studies is the ratioing of interference heating to undisturbed values. During the present tests, the external tank was tested alone so that these heating ratios could be constructed and also to confirm the data quality.

The tests were conducted in the Supersonic Wind Tunnel (A) of the von Kármán Gas Dynamics Facility (VKF) at Mach numbers 2.5, 3.5, 4.5, and 5.5 and a free-stream unit Reynolds number of 5 million per foot. Angle of attack was varied from -5 to 10 deg and sideslip angles varied from 0 to -6 deg.

2.0 APPARATUS

2.1 WIND TUNNEL

Tunnel A is a continuous, closed-circuit, variable density wind tunnel with an automatically driven flexible-plate-type nozzle and a 40- by 40-in. test section. The tunnel can be operated at Mach numbers from 1.5 to 6 at maximum stagnation pressures from 29 to 200 psia, respectively, and stagnation temperatures up to 750°R ($M_{\infty} = 6$). Minimum operating pressures range from about one-tenth to one-twentieth of the maximum at each number. The tunnel is equipped with a model injection system which allows removal of the model from the test section while the tunnel remains in operation. A schematic view of Tunnel A is presented in Fig. 1.

2.2 MODEL

The test model was a 0.0175-scale, thin skin, thermocouple-equipped model of the Rockwell International Vehicle 5 configuration of the Space Shuttle. Rockwell International fabricated the model and supplied the model drawings. A sketch of the model showing the model coordinate system and the overall full-scale dimensions is presented in Figure 2. The integrated model was composed of the orbiter vehicle, external tank, and two solid rocket booster motors that are identified in Fig. 3.

The external tank was designed with two interchangeable nose tip configurations. The two nose tip profiles are shown in Fig. 4. The smooth nose configuration in Fig. 4a is an extension of the ogive contour of the forward section of the external tank. The nipple nose configuration, Fig. 4b, has a spherical nose tip extended from the ogive contour.

The model was constructed of 17-4 PH stainless steel. The nominal skin thickness was 0.030 in. at the instrumented areas. All thermocouples were spot-welded to the inner surface of the model and the skin thickness was measured at each thermocouple location.

Boundary-layer trips were designed to be form-fitted to the orbiter and the solid rocket boosters. The orbiter and solid rocket booster trips consisted of 0.020-in.-diam stainless steel balls spot-welded to a thin, stainless steel band. The trips attached to the orbiter at an x_o/L_o of 0.04 and on the solid rocket boosters at an x_s/L_s of 0.019. The trip ring on the external tank consisted of a band of No. 36 Carborundum® grit located at an x_T/L_T of 0.069. A pictorial view of the trip ring on the external tank with the smooth nose attached is shown in Fig. 5.

The model configurations tested consisted of the external tank alone with either the smooth nose, Fig. 5, or the nipple nose, Fig. 6, installed and all protuberances removed and the integrated model with the nipple nose installed on the external tank, Fig. 3. No data were recorded for the orbiter model during this test.

2.3 INSTRUMENTATION AND MEASUREMENT PRECISION

Tunnel A stilling chamber pressure is measured with a 15-, 60-, 150-, or 300-psid transducer referenced to a near vacuum. Based on periodic comparisons with secondary standards, the uncertainty (a bandwidth which includes 95 percent of the residuals) of these transducers is estimated to be within ± 0.2 percent of reading or ± 0.015 psia, whichever is greater. Stilling chamber temperature is measured with a copper-constantan thermocouple with an uncertainty of $\pm 3^\circ\text{F}$ based on repeat calibrations.

The model temperatures were measured with iron-constantan thermocouples with an estimated uncertainty of ± 0.5 percent. There were 837 thermocouples installed on the model. A Beckman® 210 analog-to-digital converter was used in conjunction with a CDC 160-A computer to record the temperature data.

The standard Tunnel A instrumentation system is designed to record a maximum of 97 thermocouples. To more efficiently accommodate the 837 thermocouples on this test required the installation of additional equipment. A new terminal board was fabricated that allowed 291 thermocouples to be connected at one time. An existing three-position switch was incorporated that was used to select a group of 97 thermocouples to be recorded during each model injection. All the model thermocouple leads were terminated at quick-disconnect plugs. These plugs were easily interchanged with mating plugs that attached to the terminal board. In this manner, a preselected group of 291 thermocouples could be rapidly connected, and by varying this hookup it was possible to record data from all 837 thermocouples.

3.0 PROCEDURE

3.1 TEST CONDITIONS

The tests were conducted at the following nominal conditions:

M_∞	p_o , psia	T_o , °R	h_{REF} , Btu/sec-ft ² -°R	Re_∞ , ft ⁻¹
2.5	32	660	0.062	5.0×10^6
3.5	57	680	0.055	5.0×10^6
4.5	95	665	0.047	5.0×10^6
5.5	178	740	0.045	5.0×10^6

Data were obtained at angles of attack of 0, ± 5 , and 10 deg and yaw angles of 0, 3, and 6 deg. A complete test matrix with the model configurations tested is included in Table I.

Uncertainties of the basic tunnel parameters were estimated from repeat calibrations of the p_o and T_o instruments and from the repeatability and uniformity of the tunnel flow during calibrations. The parameters, p_o , T_o , and M_∞ with their uncertainties, were then used to compute the uncertainties in the other parameters dependent on these by means of the Taylor series method of error propagation.

Approximate uncertainties in tunnel flow parameters are shown as follows:

M_∞	Uncertainty (\pm), percent			
	M_∞	p_o	T_o	Re_∞
2.5	0.8	0.2	0.5	1.3
3.5	0.5	0.2	0.5	1.3
4.5	0.4	0.2	0.5	1.3
5.5	0.3	0.2	0.5	1.3

3.2 TEST PROCEDURE

The desired model attitude was established prior to injecting the model into the flow. When the model reached tunnel centerline, the model was immediately translated forward into the undisturbed tunnel flow. The thermocouple outputs were scanned approximately 20 times per second starting prior to model injection into the airstream and continuing about 4 sec after the model reached the tunnel centerline. After each injection, the model was cooled to an isothermal state using high-pressure air.

3.3 DATA REDUCTION AND PRECISION

The reduction of thin skin thermocouple data normally involves only the calorimetric heat balance which in coefficient form is:

$$h(T_o) = wbc_p \frac{dT_w/dt}{T_o - T_w} \quad (1)$$

Radiation and conduction losses are neglected in this heat balance, and data reduction simply requires evaluation of dT_w/dt from the temperature-time data and determination of model material properties. For the present tests, radiation effects were negligible; however, conduction effects can be significant in several regions of the models. To permit identification of these regions, and to improve evaluation of the data, the following procedure was used.

Separation of variables and integration of Eq. (1) assuming constant w , b , c_p , and T_o yields

$$\frac{h(T_o)}{w b c_p} (t - t_i) = \ln \left[\frac{T_o - T_{w_i}}{T_o - T_w} \right] \quad (2)$$

Differentiation of Eq. (2) with respect to time gives

$$\frac{h(T_o)}{w b c_p} = \frac{d}{dt} \ln \left[\frac{T_o - T_{w_i}}{T_o - T_w} \right] \quad (3)$$

Since the left side of Eq. (3) is a constant, plotting versus time will give a straight line if conduction is negligible. Thus, deviation from a straight line can be interpreted as a conduction effect.

The data were evaluated in this manner, and generally a linear portion of the curve was used for all thermocouples. A linear least-squares curve fit of $\ln[(T_o - T_{w_i})/(T_o - T_w)]$ versus time was applied to the data. The data from a typical thermocouple are presented in Fig. 7. The value of the initial slope is high when the model is located on the tunnel centerline in the rear test section. As the model is translated forward out of this region into the undisturbed tunnel flow a new linear slope is established that is the desired value of $d/dt \ln[(T_o - T_{w_i})/(T_o - T_w)]$. Generally, for all thermocouples with a value of x_T/L_T less than or equal to 0.05 the curve fit was started at the time the model reached the tunnel centerline. The curve fit for thermocouples with a value of x_T/L_T greater than 0.05 and less than or equal to 0.1 started 1.0 sec after the model reached centerline. The curve fit for the remaining thermocouples started 2.0 sec after

centerline to ensure that the model was clear of any disturbance in the aft part of the test section. The curve fit extended for a time span, which was a function of the heating rate, as shown below:

<u>Range</u>	<u>Number of Points</u>
$dTw/dt > 32$	5
$16 < dTw/dt \leq 32$	7
$8 < dTw/dt \leq 16$	9
$4 < dTw/dt \leq 8$	13
$2 < dTw/dt \leq 4$	17
$1 < dTw/dt \leq 2$	25
$dTw/dt < 1$	41

The above time spans were adequate to keep the evaluation of the right side of Eq. (3) within the linear region. The linearity of the fit was substantiated by visual inspection of the cases in question. Strictly speaking, the value of c_p for the material was not constant, as assumed, and the following relation:

$$c_p = 0.0797 + (5.556 \times 10^{-5})T, \text{ (17-4 PH stainless steel)} \quad (4)$$

was used with the value of T_w at the midpoint of the curve fit. The maximum variation of c_p over the curve fit was less than 1.2 percent. The value of density used for 17-4 PH stainless steel was

$$w = 480.0 \text{ lbm/ft}^3$$

For this test, the wall recovery temperature was selected as $0.9 T_o$ to conform with previous shuttle heat-transfer data. The heat balance becomes:

$$h(0.9T_o) = w b c_p \frac{dT_w/dt}{0.9T_o - T_w} \quad (5)$$

Estimated uncertainties for the individual terms in Eq. (5) were used in the Taylor series method of uncertainty propagation to obtain the uncertainty in the heat-transfer coefficient as given below:

<u>$h(0.9 T_o)$</u>	<u>Uncertainty, percent</u>
10^{-4}	14
10^{-3}	13
10^{-2}	11.5

These estimated uncertainties are based on a T_w of 540°R and a value of T_w/T_o equal to 0.818.

4.0 RESULTS AND DISCUSSION

4.1 EXTERNAL TANK ALONE

During the initial phase of the test, data were obtained on the external tank alone. These data formed the baseline for comparison with the data obtained with the integrated model and provided an indication of overall data quality. Figure 8 is a comparison of 0 and 180-deg ray heat-transfer-rate distributions on the external tank with the smooth nose. Calculated values of laminar and turbulent heating rates for this configuration are also presented in Fig. 8a for zero angle-of-attack. The method used to calculate these heating rates is that of Refs. 2, 3, and 4 with pressures calculated from modified Newtonian theory. The measured heat-transfer rates ahead of the boundary-layer trip location, $x_T/L_T = 0.069$, are in good agreement with the calculated laminar rates. The trip effectiveness is evident with the transition to the turbulent level completed at a value of x_T/L_T of 0.08. The agreement of the measured and calculated turbulent heat-transfer rates is very good with the exception of two regions. In the region between x_T/L_T of 0.2 and 0.35, the heating rates indicate that the flow may be relaminarizing. This same trend was noted consistently throughout the test data. An investigation of relaminarization under compressible flow conditions is reported by Nash-Webber in Ref. 5. In this work, a boundary-layer edge acceleration parameter and a momentum thickness Reynolds number based on edge conditions are used to correlate relaminarization.

Computations of these parameters for the x_T/L_T location of 0.25 confirm the probable occurrence of relaminarization for the present tests. The second region where the measured and calculated heat-transfer rates are not in agreement is around x_T/L_T of 0.9. This could be caused by an upstream effect of the expansion at the rear of the tank. The tangent point for the dome at the rear of the tank is located at x_T/L_T of 0.93.

The windward and leeward centerline heat-transfer-rate distributions for the external tank with the smooth nose configuration are presented in Fig. 8b for a 10-deg angle of attack. The transition to turbulent heating is again evident between x_T/L_T of 0.06 to 0.08. Windward centerline heating rate measurements are in general agreement with calculated turbulent values. Note that the lee side heating rates at x_T/L_T values greater than 0.6 equal the zero angle-of-attack case. This is indicative of a vortex interaction phenomenon as observed on other configurations (see Ref. 6, for example).

A comparison of axial heat-transfer-rate distributions on the external tank at zero angle of attack both with and without the boundary-layer trip is presented in Fig. 9 for the nipple nose configuration. It is noted that the distribution with the boundary-layer trip is essentially the same as the clean distribution. Upon closer examination it is evident that transition to the turbulent distribution occurs between x_T/L_T of 0.02 and 0.03. Since the boundary-layer trip was located at 0.069, these data indicate that the boundary layer is tripped by the shock wave/boundary-layer interaction generated by the nipple nose.

Also shown in Fig. 9 is a fairing of the smooth nose data from Fig. 8a. It is apparent that the nipple nose has essentially no effect on the heating rates downstream of $x_T/L_T = 0.1$.

Zero angle-of-attack axial heat-transfer-rate distributions on the external tank with the nipple nose are shown for Mach numbers 2.5, 3.5, 4.5, and 5.5 in Fig. 10. The calculated smooth nose turbulent heating rates are included for each Mach number. The agreement between the measured and calculated values is, in general, very good.

4.2 INTEGRATED MODEL

The axial heat-transfer-rate distributions on the leeward centerline of the external tank for the integrated model are presented for Mach numbers 3.5, 4.5, and 5.5 in Fig. 11. Data fairings for the external tank alone are included to provide a baseline for comparing the interference heating to undisturbed heating rates. Peak heating resulting from interaction with the orbiter occurred at an $x_T/L_T \approx 0.445$. The ratio of the peak heating to the undisturbed heating value is 10 for Mach number 3.5 and 5.5 and 12 for Mach number 4.5. Figure 12 presents shadowgraph photographs of the flow on the external tank with the nipple nose and on the integrated model, respectively. Figure 12b shows the interaction of the orbiter bow shock with the external tank, and the region of peak heating shown in Fig. 11 is indicated on the photograph.

The heat-transfer-rate distribution on the side of the external tank resulting from the interaction of the solid rocket booster is shown in Fig. 13. The peak heating occurred at an x_T/L_T of 0.35. The ratio of the peak heating to the undisturbed heating value is 22. The bow shock from the solid rocket booster can be seen in Fig. 12b.

5.0 CONCLUDING REMARKS

5.1 EXTERNAL TANK ALONE

The external tank was tested with two nose tip configurations to obtain undisturbed heat-transfer-rate distributions. These distributions were used to confirm the data quality

and to provide a comparative baseline for the heating rates from the integrated model. The more significant comments concerning these tests are:

1. The measured heating rate distributions were, in general, in good agreement with calculated turbulent heat-transfer-rate distributions.
2. The nipple nose configuration on the external tank effectively tripped the boundary layer to turbulent conditions without the addition of artificial roughness.
3. A trend toward relaminarization was noted on the external tank at x_T/L_T of 0.25 where the nose ogive mates with the cylindrical body.

5.2 INTEGRATED MODEL

The integrated model was tested to investigate heating rates during the ascent phase of the mission. Because of the complex shock interaction, no calculated heating rate values were available for comparison. Instead, the peak heating values obtained on the external tank were compared with the undisturbed heating values. The peak heating rate on the leeward centerline of the external tank occurred at an x_T/L_T of 0.44 and ranged between 10 to 12 times the undisturbed value. No noticeable Mach number effect in the peak heating was indicated. A peak heating ratio of 22 occurred on the side of the external tank, $\phi_T = 90$ deg, at an x_T/L_T of 0.35.

REFERENCES

1. Keyes, J. Wayne and Hains, Frank D. "Analytical and Experimental Studies of Shock Interference Heating in Hypersonic Flows." NASA TN D-7139, May 1973.
2. DeJarnette, Fred R. "Calculation of Inviscid Surface Streamlines on Shuttle Type Configurations, Part I - Description of Basic Method." NASA CR-111921, August 1971.
3. DeJarnette, Fred R. and Jones, Michael H. "Calculation of Inviscid Surface Streamlines and Heat Transfer On Shuttle Type Configurations, Part 2 - Description of Computer Program." NASA CR-111922, August 1971.
4. DeJarnette, Fred R. "Calculation of Heat Transfer on Shuttle-Type Configurations Including the Effects of Variable Entropy at the Boundary Layer Edge." NASA CR-112180, October 1972.

5. Nash-Webber, J. L. "Wall Shear-Stress and Laminarization in Accelerated Turbulent Compressible Boundary-Layers." MIT Gas Turbine Lab. Report No. 94, April 1968.
6. Hefner, Jerry N. "Lee-Surface Heating and Flow Phenomena on Space Shuttle Orbiters at Large Angles of Attack and Hypersonic Speeds." NASA TN D-7088, November 1972.

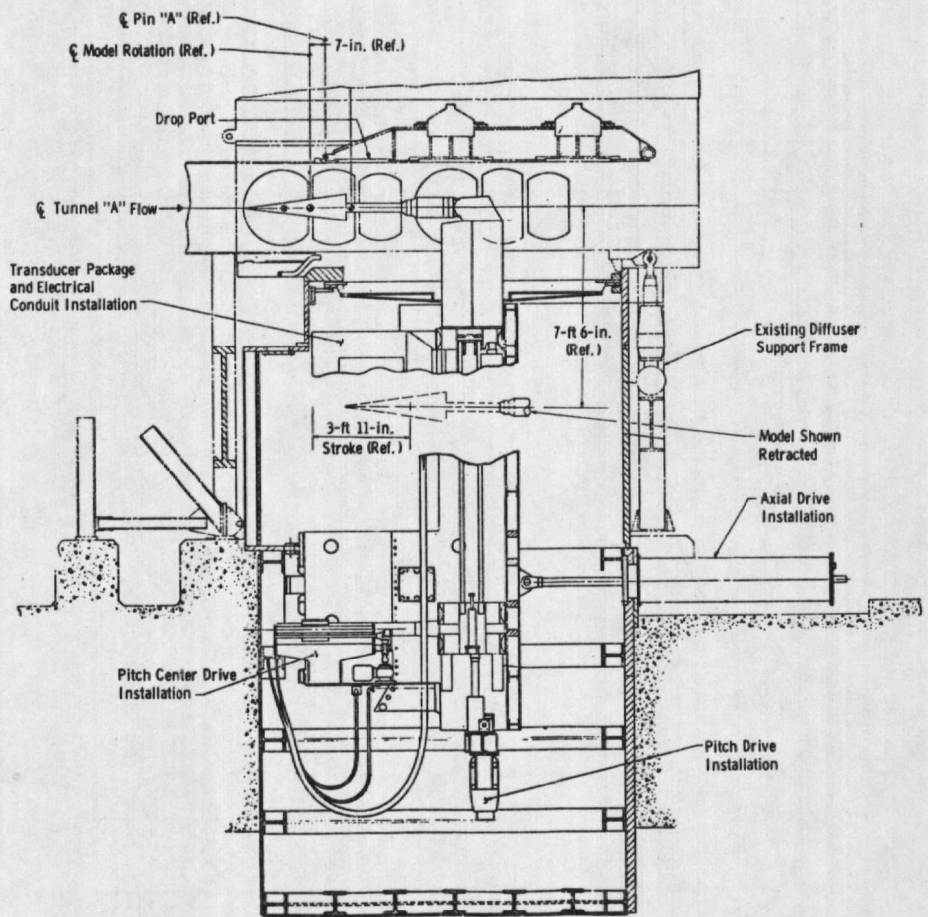
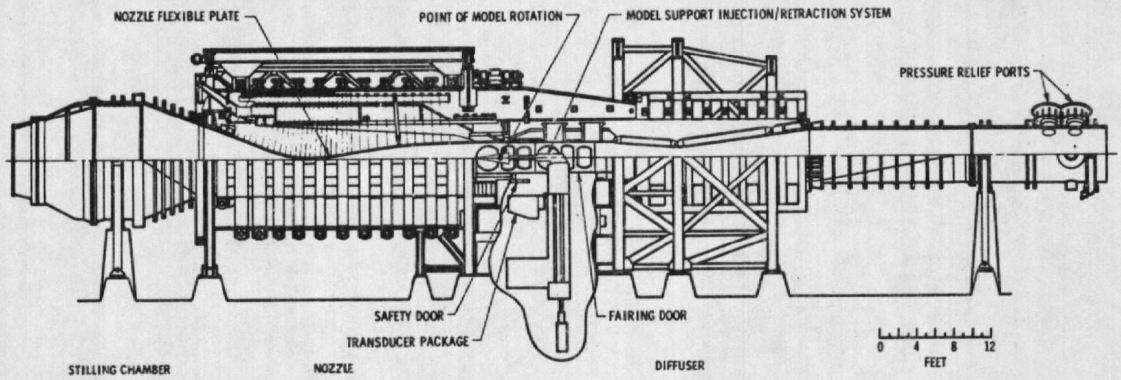


Figure 1. Schematic view of Tunnel A.

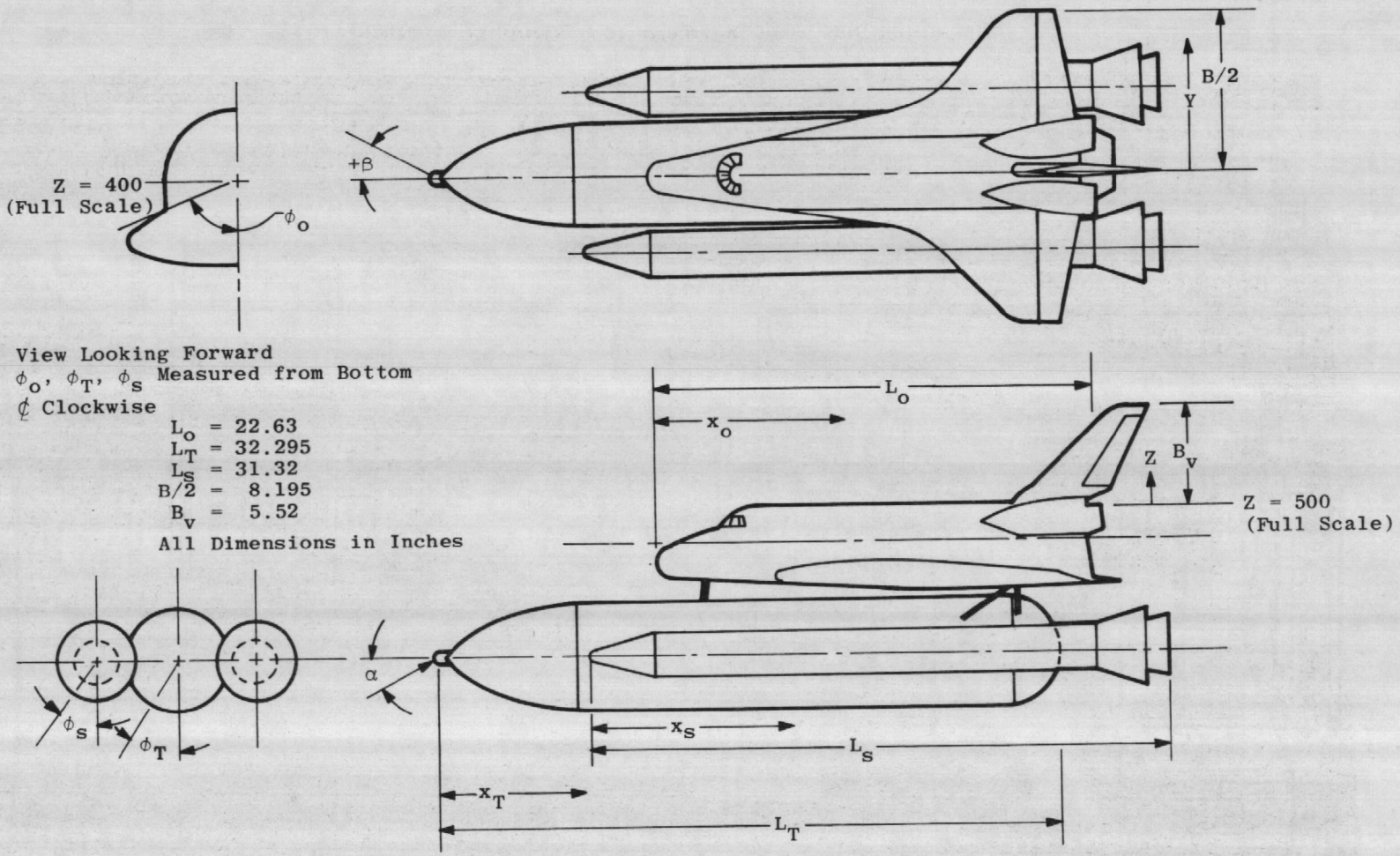


Figure 2. Model sketch.

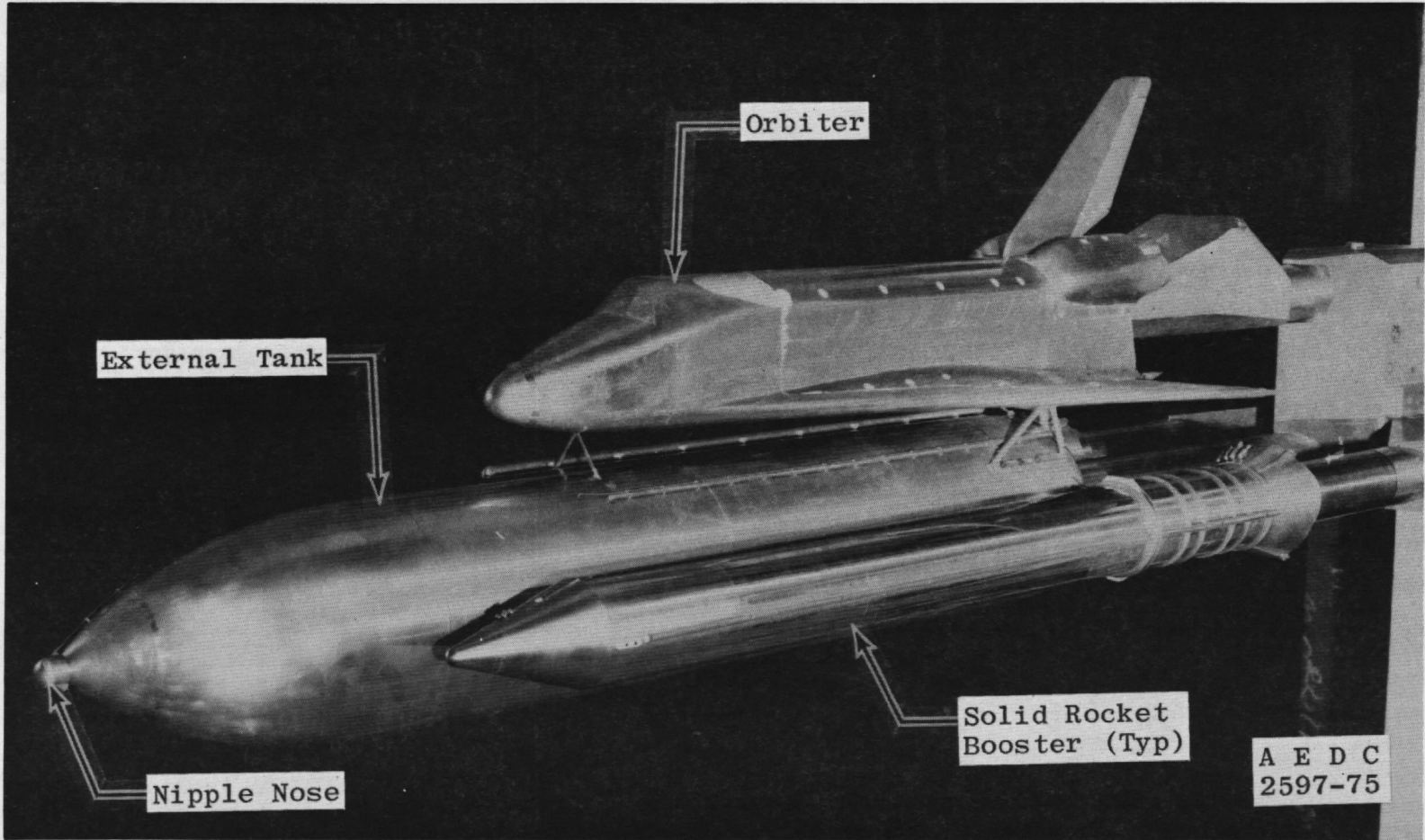


Figure 3. Photograph of integrated space shuttle model.

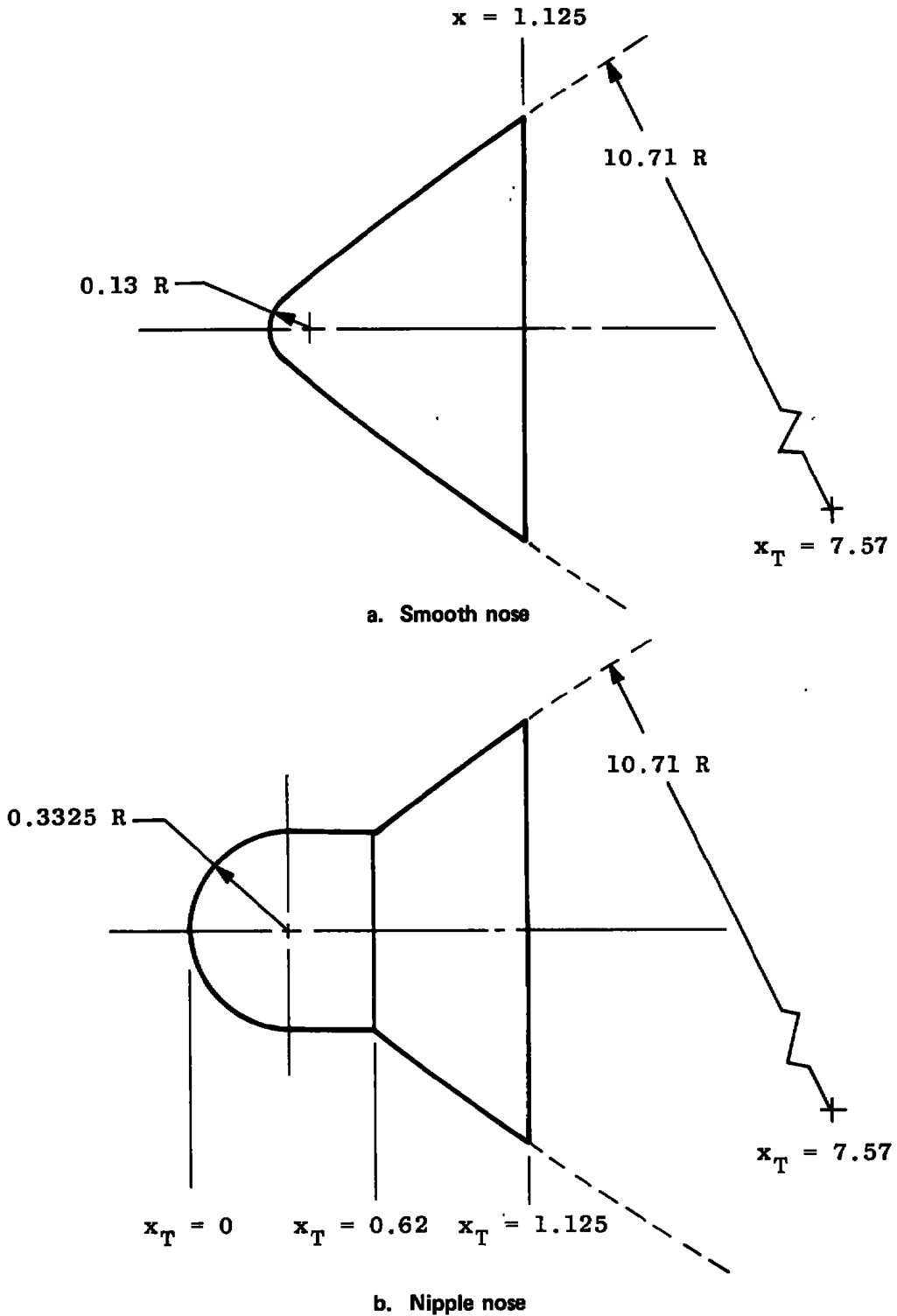


Figure 4. External tank nose tip configurations.

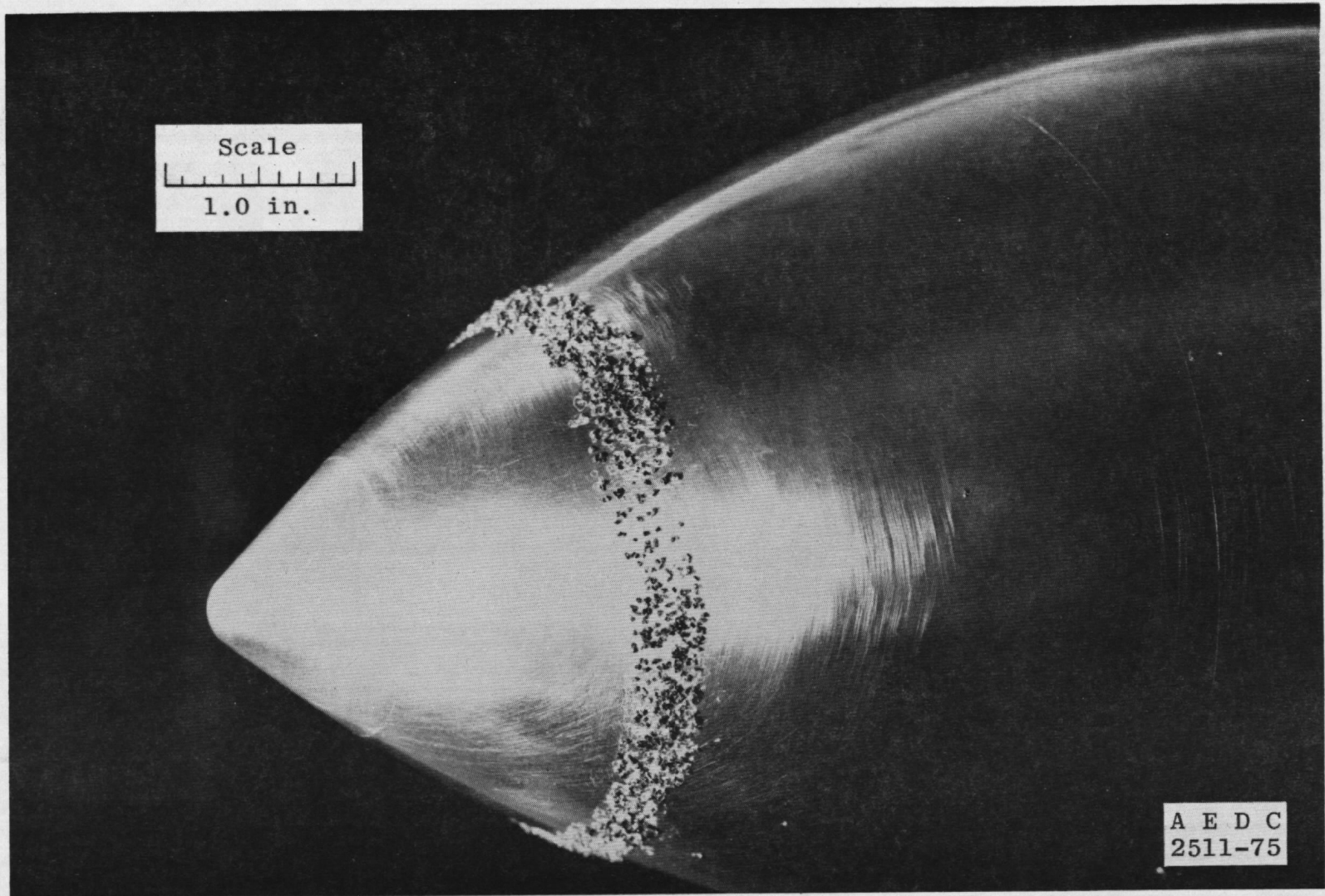


Figure 5. Photograph of the boundary-layer trip on the external tank.

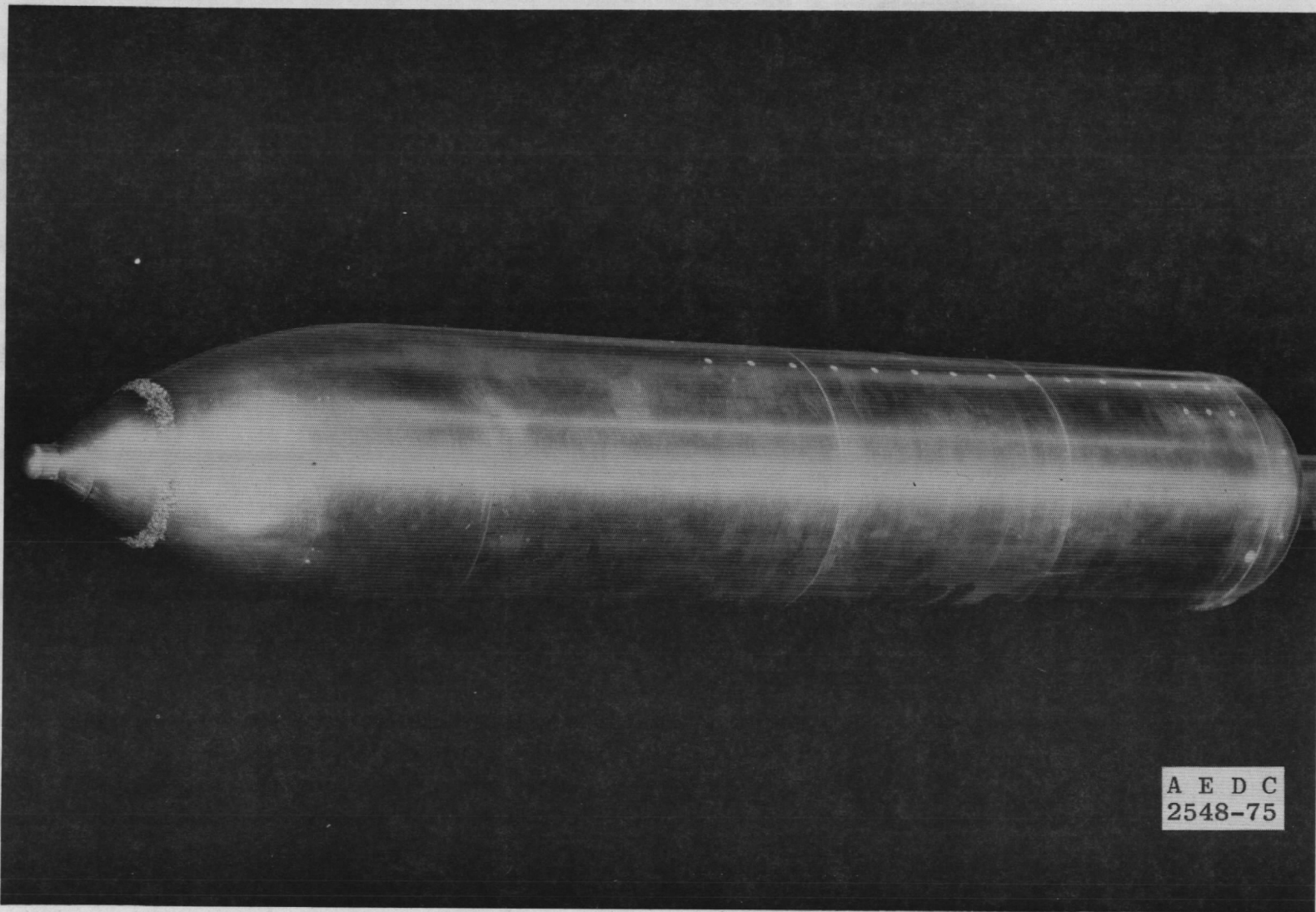


Figure 6. Photograph of external tank with nipple nose.

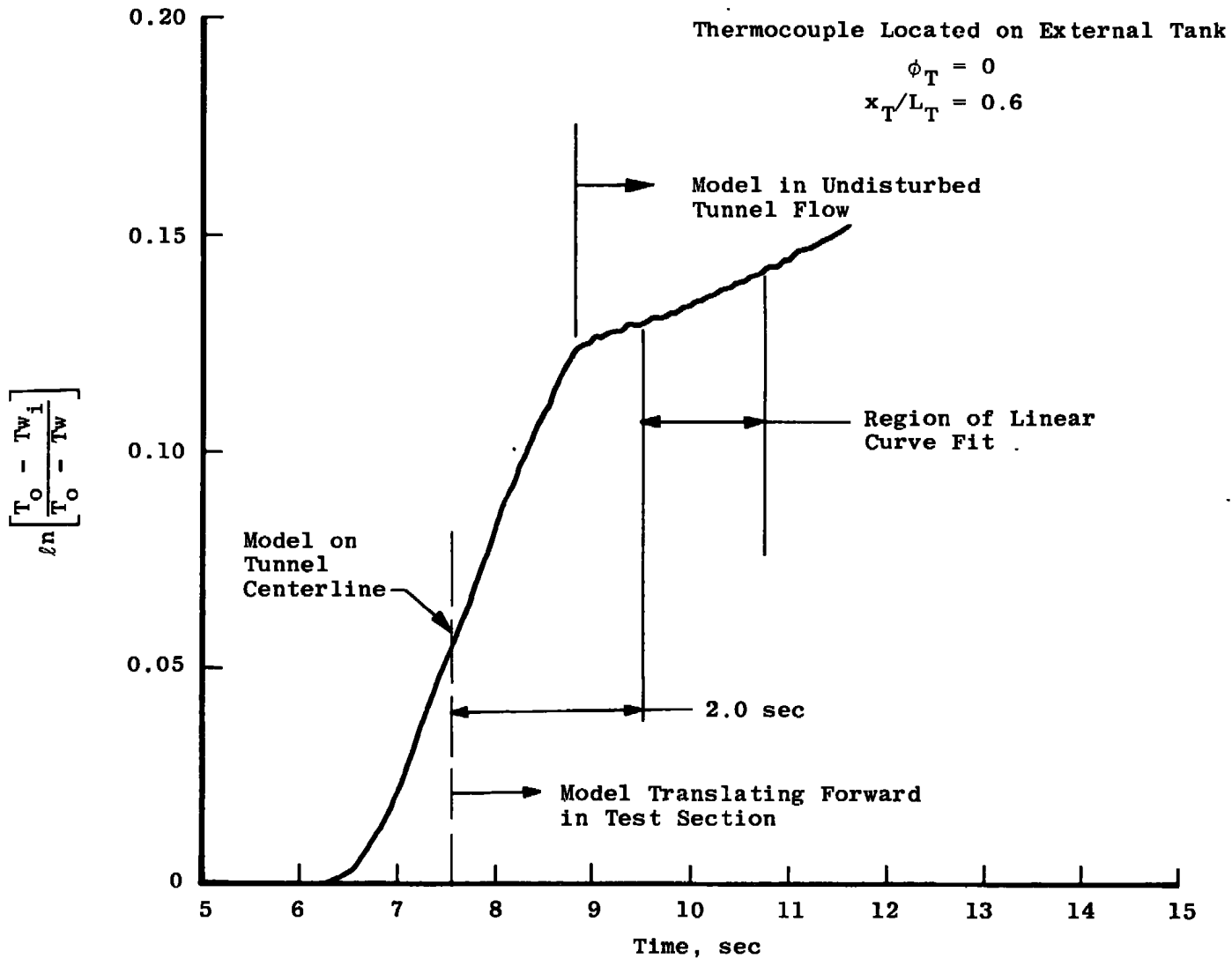


Figure 7. Typical data for a thermocouple.

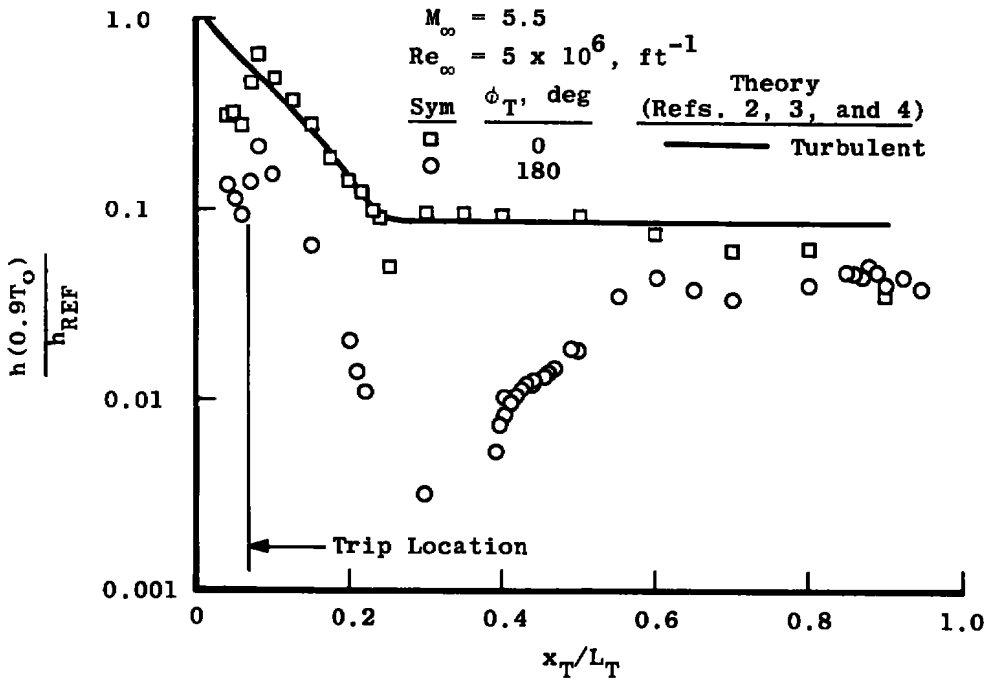
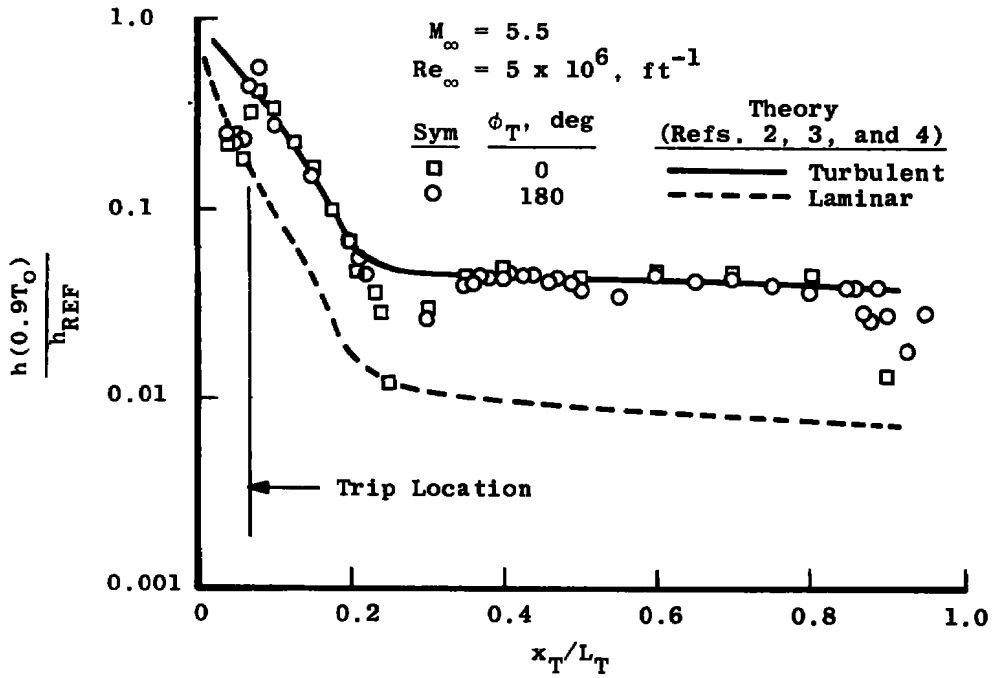


Figure 8. Heat-transfer-rate distributions for external tank with smooth nose.

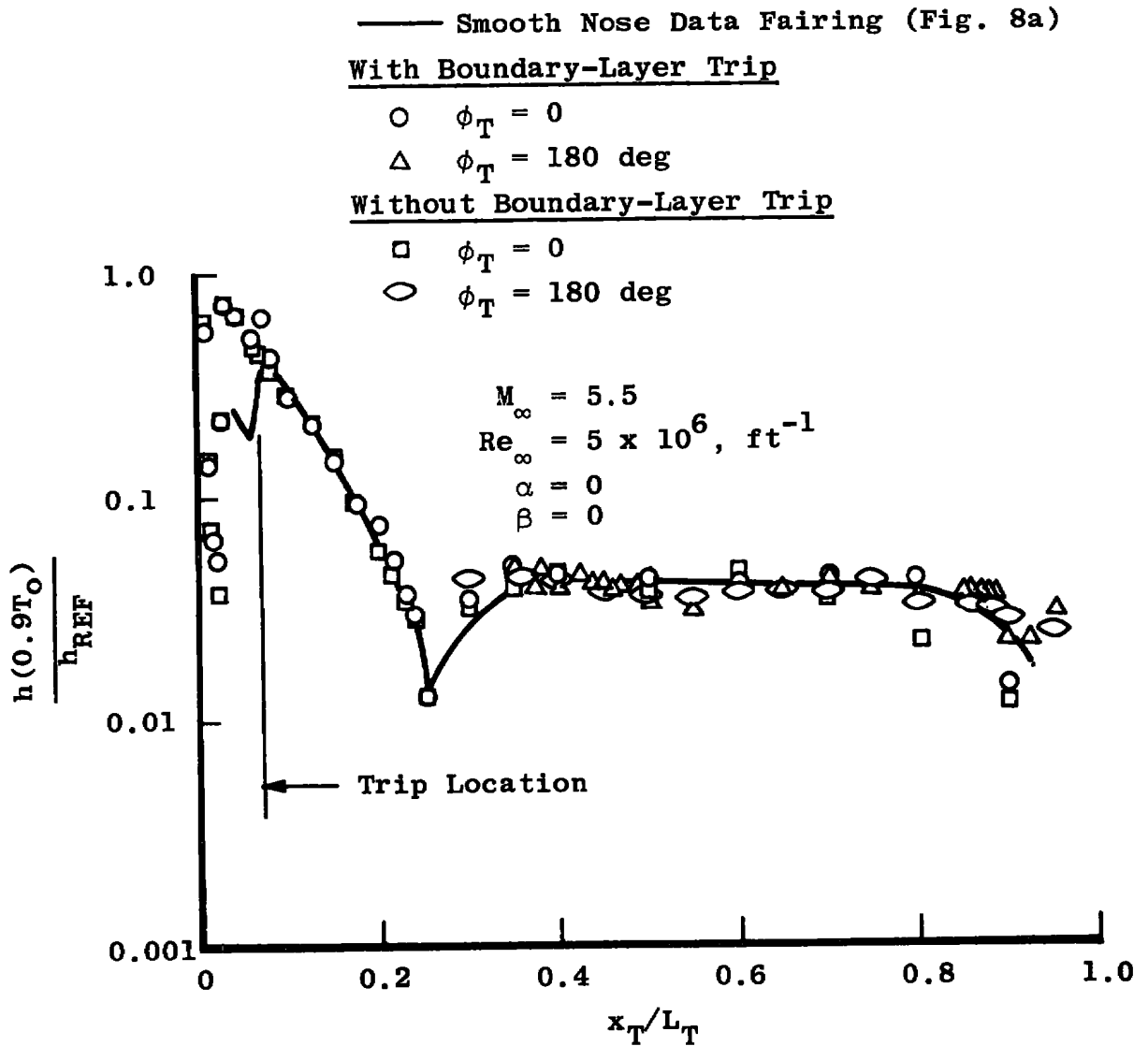


Figure 9. Influence of boundary-layer trip on the heat-transfer-rate distribution of the external tank with nipple nose.

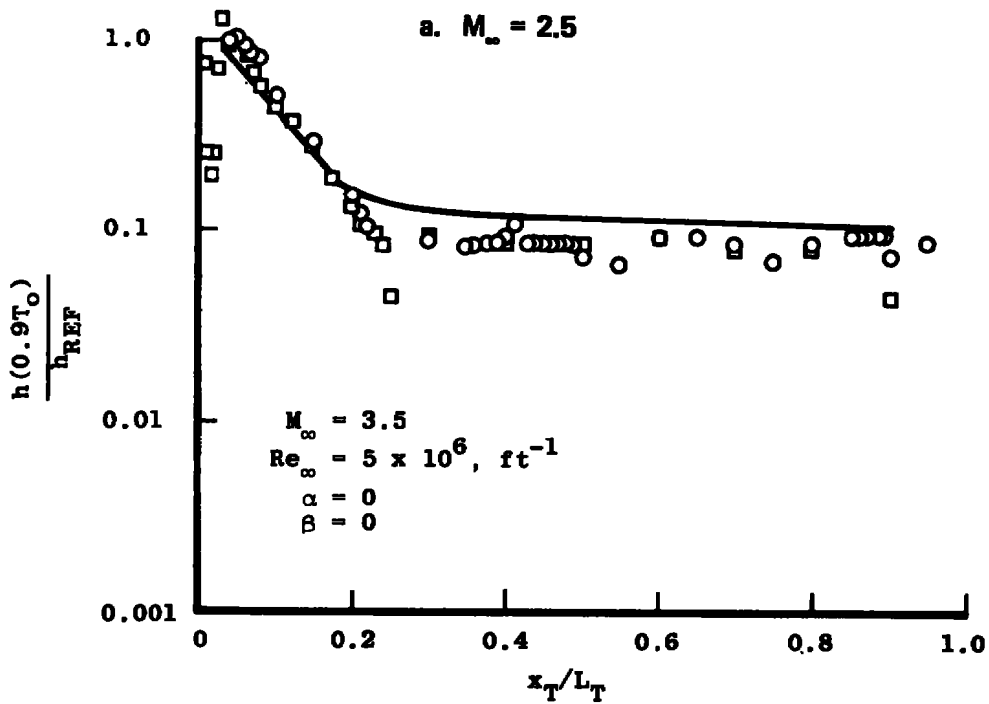
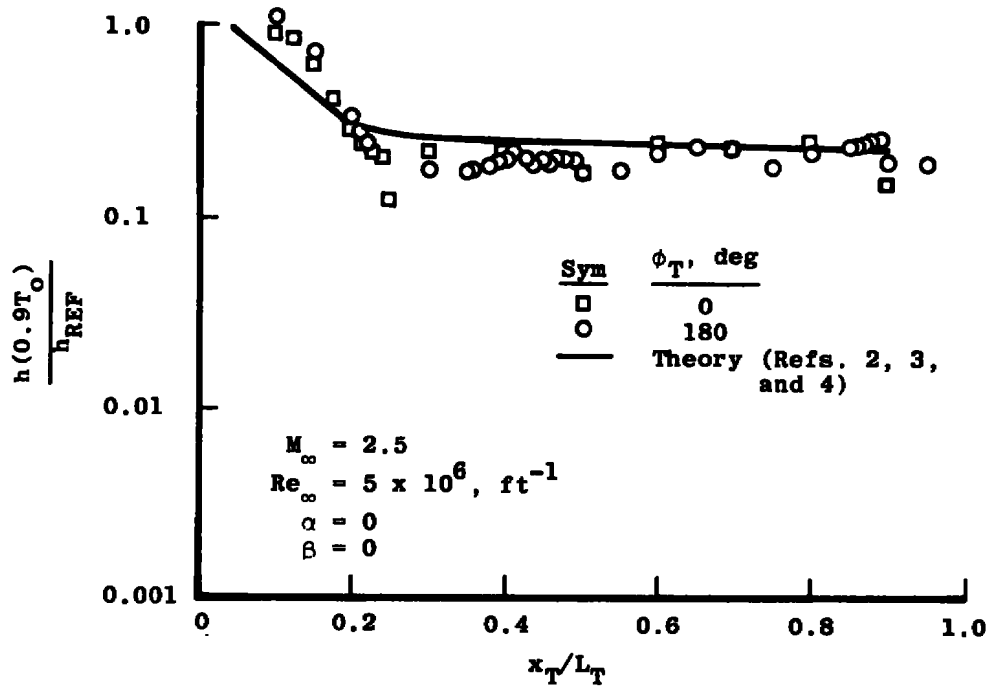
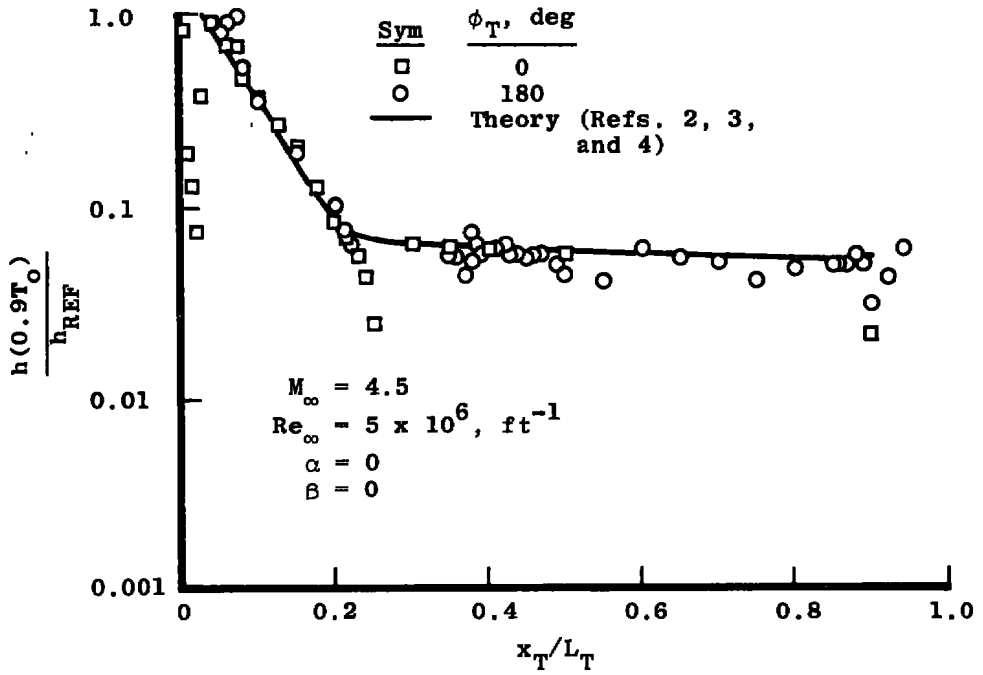
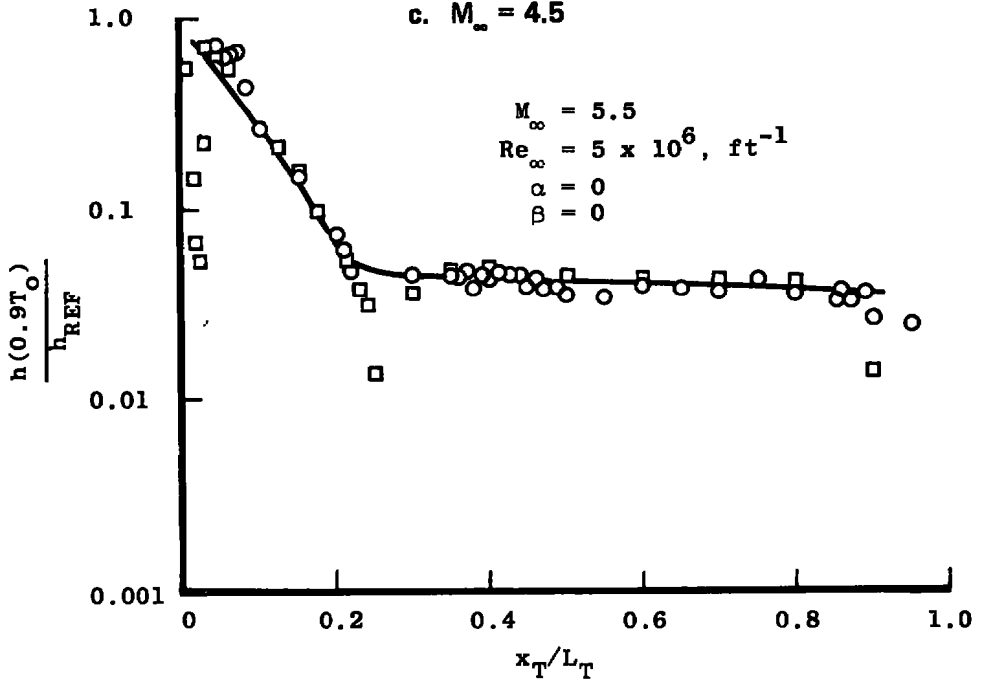


Figure 10. Heat-transfer-rate distributions for the external tank with nipple nose.

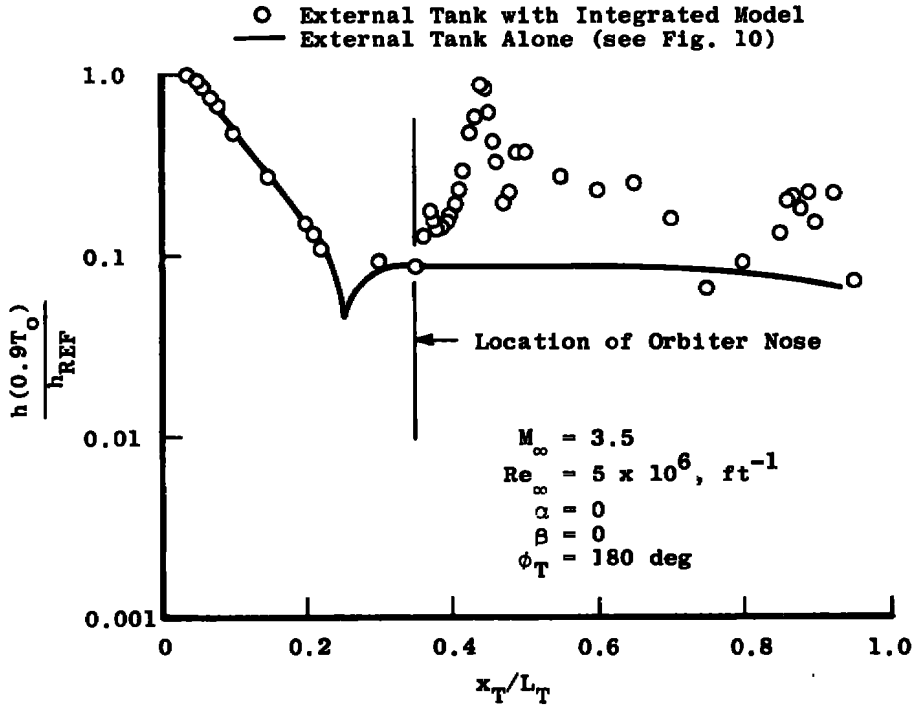


c. $M_\infty = 4.5$

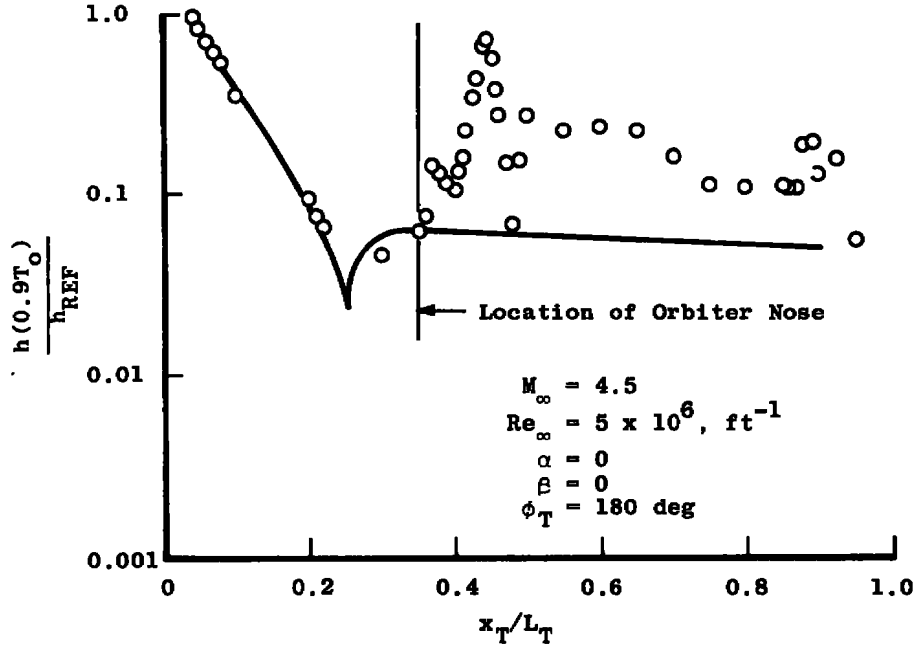


d. $M_\infty = 5.5$

Figure 10. Concluded.

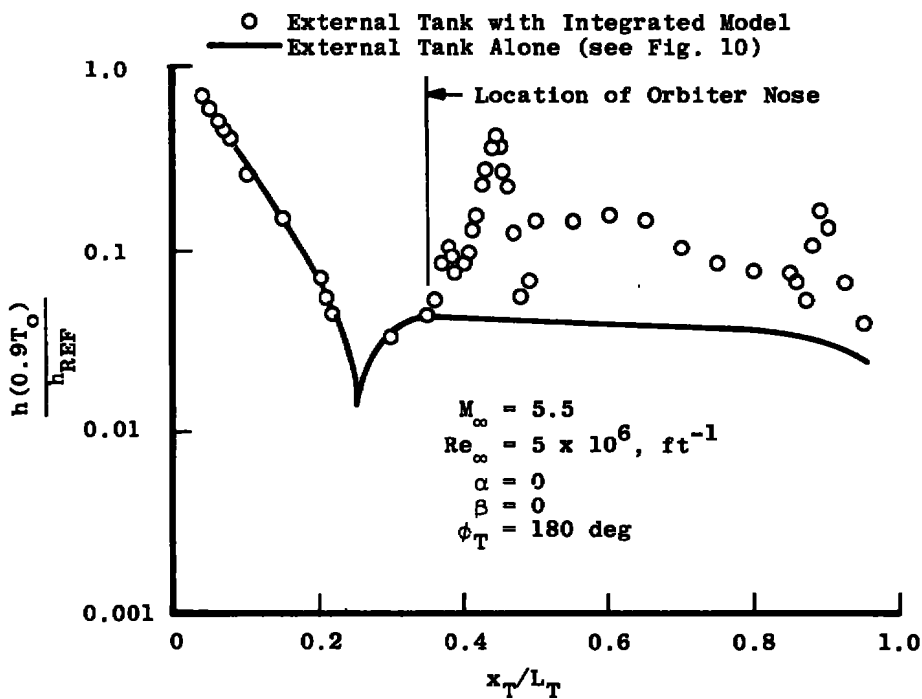


a. $M_\infty = 3.5$

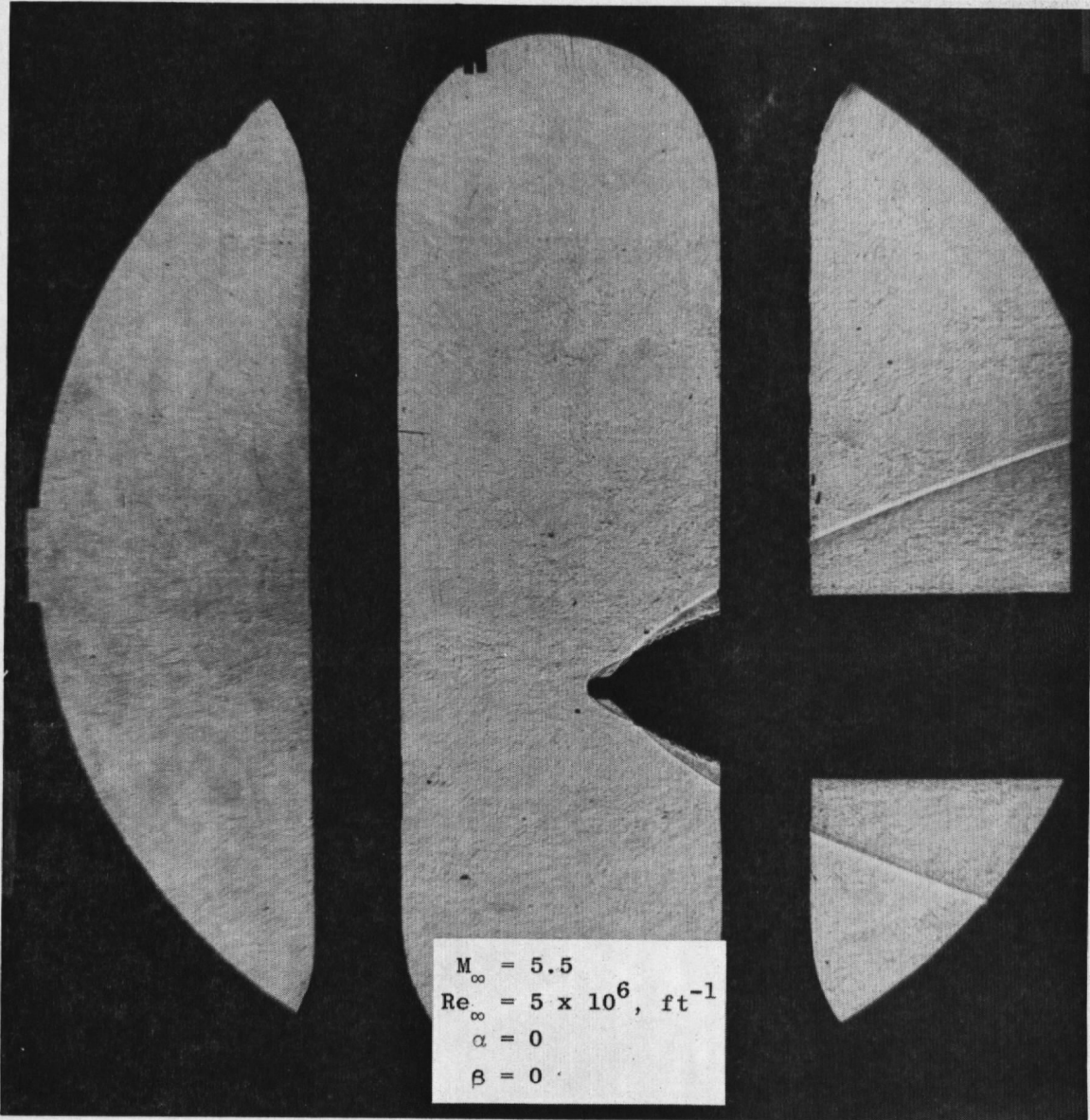


b. $M_\infty = 4.5$

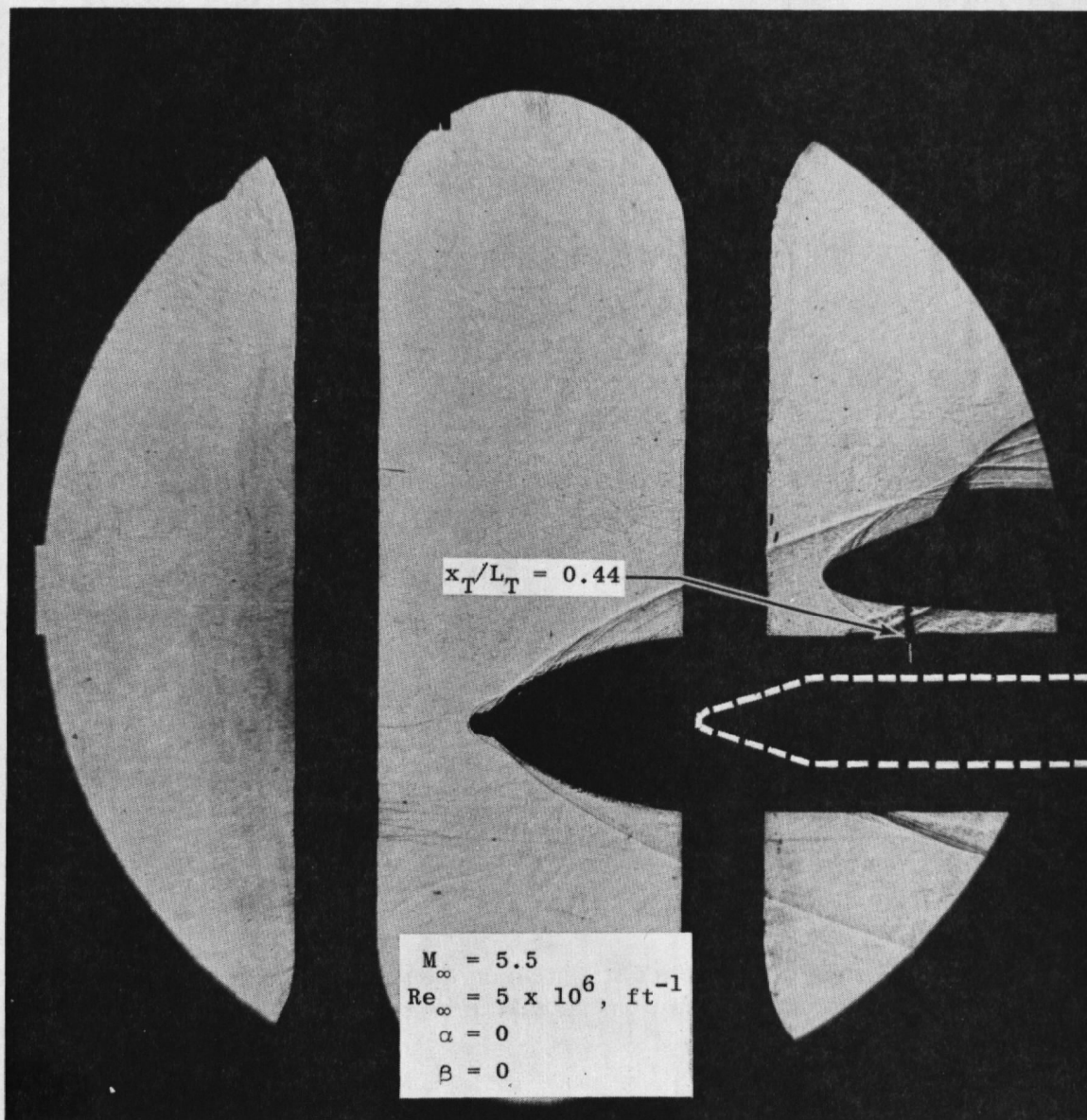
Figure 11. Heat-transfer-rate distributions for the external tank with interaction from the orbiter.



c. $M_\infty = 5.5$
 Figure 11. Concluded.



a. External tank with nipple nose
Figure 12. Model flow-field shadowgraphs.



b. Integrated shuttle model
Figure 12. Concluded.

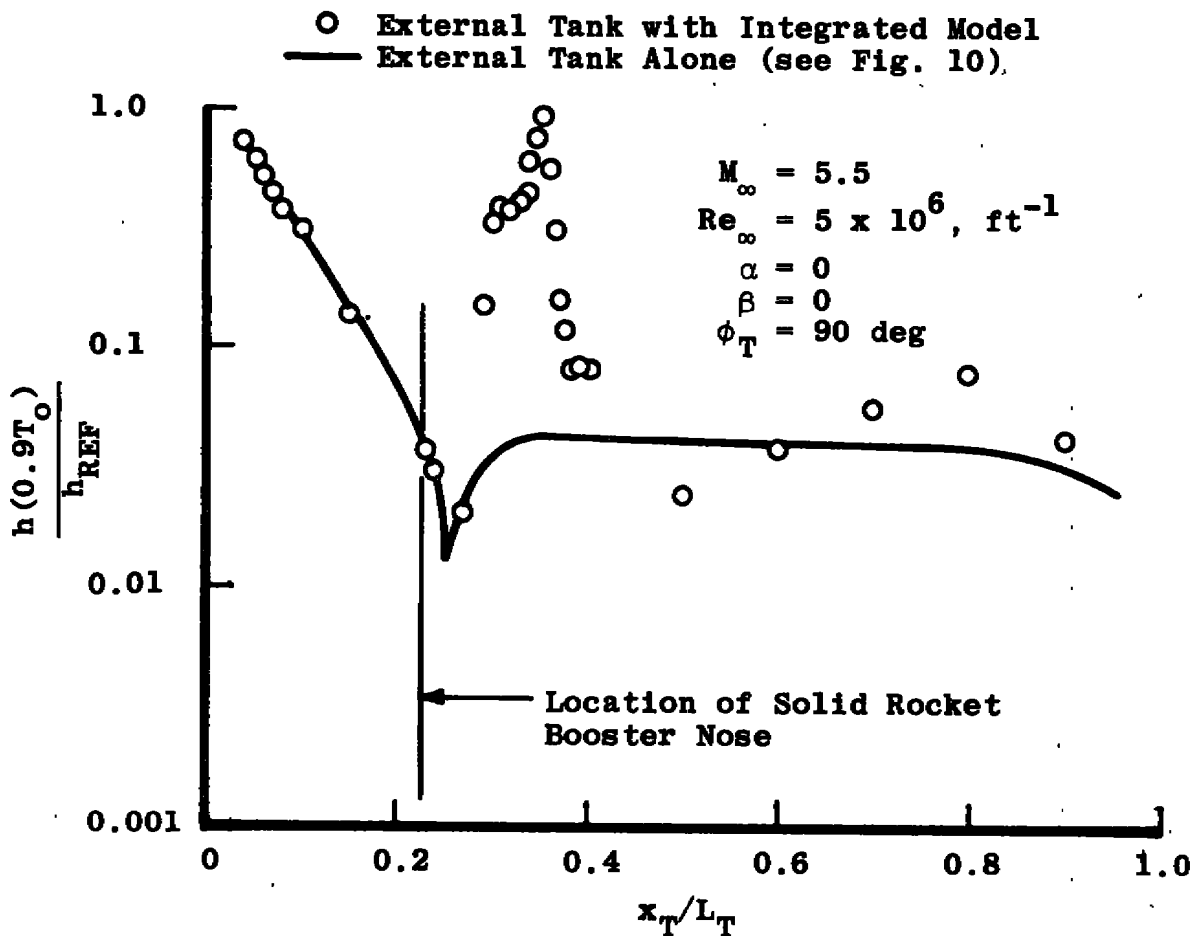


Figure 13. Heat-transfer-rate distribution on the side of the external tank with interaction from the solid rocket booster.

Table 1. Test Matrix

M_∞	Model Configuration	External Tank Nose Configuration	External Tank Trip	α , deg	β , deg	
5.5	External Tank Alone	Smooth	Clean	0	0	
			No. 36 Grit	0	0	
				5	0, -3, -6	
		10	0, -3, -6			
		Nipple	Clean	0	0	
			No. 36 Grit	5	0	
	10			0, -3, -6		
	Integrated Model (Data Obtained Only on External Tank)	Nipple	Clean	-5	0, -3, -6	
			0	0		
			5	0, -3, -6		
10	0, -3, -6					
Integrated Model (Data Obtained Only on Solid Rocket Booster)	Nipple	Clean	0	0		
4.5	External Tank Alone	Smooth	No. 36 Grit	0	0	
			Nipple	Clean	0	0
				5	0	
		No. 36 Grit	0	0		
			5	0, -3, -6		
			10	0, -3, -6		
	Integrated Model (Data Obtained Only on External Tank)	Nipple	Clean	-5	0, -3, -6	
			0	0		
			5	0, -3, -6		
	10	0, -3, -6				
Integrated Model (Data Obtained Only on Solid Rocket Booster)	Nipple	Clean	0	0		
3.5	External Tank Alone	Nipple	Clean	0	0	
			No. 36 Grit	0	0	
				5	0, -3, -6	
		10	0, -3, -6			
		Integrated Model (Data Obtained Only on External Tank)	Nipple	Clean	0	0
				No. 36 Grit	-5	0, -3, -6
	5				0, -3, -6	
	10	0, -3, -6				
	Integrated Model (Data Obtained Only on Solid Rocket Booster)	Nipple	Clean	0	0	
	2.5	External Tank Alone	Nipple	No. 36 Grit	0	0
5					0, -3, -6	
10					0, -3, -6	

NOMENCLATURE

b	Model skin thickness, ft
B	Model wing span, in. (see Fig. 2)
B _v	Vertical tail span with origin at Z = 500. in. (full scale) (see Fig. 2)
c _p	Specific heat, Btu/lbm-°R
h(T _o)	Heat-transfer coefficient based on T _o , $\frac{\dot{q}}{T_o - T_w}$, $\frac{\text{Btu}}{\text{ft}^2\text{-sec}\cdot^\circ\text{R}}$
h(0.9T _o)	Heat-transfer coefficient based on 0.9T _o , $\frac{\dot{q}}{(0.9T_o) - T_w}$, $\frac{\text{Btu}}{\text{ft}^2\text{-sec}\cdot^\circ\text{R}}$
h _{REF}	Reference heat-transfer coefficient based on Fay-Ridell theory and a 1-ft nose radius scaled to the model scale (0.0175 ft)
L _o	Axial length of orbiter model, in. (see Fig. 2)
L _s	Axial length of solid rocket booster model, in. (see Fig. 2)
L _T	Axial length of external tank model, in. (see Fig. 2)
M _∞	Free-stream Mach number
p _o	Tunnel stilling chamber pressure, psia
\dot{q}	Heat-transfer rate, Btu/ft ² -sec
Re	Free-stream unit Reynolds number, ft ⁻¹
T _o	Tunnel stilling chamber temperature, °R
T _w	Model wall temperature, °R
t	Time, sec
w	Model skin density, lbm/ft ³
x _o	Longitudinal coordinate with origin at the orbiter model nose, in. (see Fig. 2)
x _s	Longitudinal coordinate with origin at the solid rocket booster model nose, in. (see Fig. 2)

x_T	Longitudinal coordinate with origin at the external tank model nose, in. (see Fig. 2)
Y	Lateral coordinate, in. (see Fig. 2)
Z	Vertical coordinate, in. (see Fig. 2)
α	Angle of attack, deg
β	Angle of sideslip, equal to negative yaw angle, deg (see Fig. 2)
ϕ_o	Angular measurement on orbiter model, deg (see Fig. 2)
ϕ_s	Angular measurement on solid rocket booster, deg (see Fig. 2)
ϕ_T	Angular measurement on external tank, deg (see Fig. 2)

SUBSCRIPTS

i	Initial conditions
-----	--------------------